J|A|C|S ARTICLES

Published on Web 10/15/2009

A Reliable Quantum-Chemical Protocol for the Characterization of Organic Mixed-Valence Compounds

Manuel Renz,[†] Kolja Theilacker,[†] Christoph Lambert,[‡] and Martin Kaupp*[,†]

Institut für Anorganische Chemie and Institut für Organische Chemie, Universität Würzburg, Am Hubland, D-97074 Würzburg, Germany

Received August 21, 2009; E-mail: kaupp@mail.uni-wuerzburg.de

Abstract: Structures, dipole moments, electron-transfer barriers, and spin density distributions of a series of mixed-valent bistriarylamin radical cations have been studied systematically by hybrid density functional methods with variable exact-exchange admixture combined with a continuum solvent model. The chosen systems differ in their bridging units and are all relatively close, from both sides, to the class II/III borderline of the Robin−Day classification of mixed-valence systems. Solvent effects are found to have a dramatic influence on the localized vs delocalized character of these cations. While gas-phase calculations or computations in a nonpolar solvent place all systems on the delocalized class III side, a more polar solvent like acetonitrile enables observation of symmetry breaking and charge localization with moderate exact-exchange admixtures in a hybrid functional for the systems on the class II side (with diphenylbutadiyne and diphenylethyne bridges). In contrast, the cations with the shortest bridges (phenylene, biphenylene) are characterized as class III. The comparison of computed intervalence charge-transfer excitation frequencies with experiment confirms the system with the diphenylbutadiyne bridge, and probably the system with the diphenylethyne bridge, to be class II, whereas in the dichloromethane solvent employed for spectroscopic measurements, the two other systems are on the class III side. Nonstandard hybrid density functional calculations with 35% Hartree−Fock-like exchange combined with continuum solvent models are suggested as a practical protocol for the quantum-chemical characterization of organic mixed-valence systems. This approach should allow closer examinations and provides a basis for the evaluation of other computational methods.

1. Introduction

Mixed valence (MV) compounds are widely used as model systems to study basic electron-transfer (ET) processes.[1−4] These systems usually consist of at least two redox centers with different oxidation number connected by a bridge, for example, M^+-B-M. The bridges may be either saturated or unsaturated. In inorganic MV compounds, the redox centers usually are ligand-surrounded transition metals, whereas in organic MV compounds, the redox centers often are more extended π-systems such as hydrazines,[5−8] bis(alkoxy)benzene,[9,10] tetrathiafulvalene,[11−13] or triarylamines.[14−28] Particularly the latter attracted considerable interest during the past 10 years. Essentially two parameters govern the ground and first excited potential energy surface of a MV compound with two identical redox centers (see Figure 1), the reorganization energy λ (which is made up

[†] Institut für Anorganische Chemie.
[‡] Institut für Organische Chemie.

(1) Launay, J.-P. *Chem. Soc. Rev.* **2001**, *30*, 386.
(2) Hush, N. S. In *Mixed-Valence Compounds*; Brown, D. B., Ed.; D. Reidel Publishing Company: Dordrecht, 1980.
(3) Richardson, D. E.; Taube, H. *Coord. Chem. Rev.* **1984**, *60*, 107.
(4) Nelsen, S. F.; Ismagilov, R. F.; Trieber, D. A. *Science* **1997**, *278*, 846.
(5) Nelsen, S. F.; Konradsson, A. E.; Teki, Y. *J. Am. Chem. Soc.* **2006**, *128*, 2902.
(6) Nelsen, S. F.; Ismagilov, R. F.; Gentile, K. E.; Powell, D. R. *J. Am. Chem. Soc.* **1999**, *121*, 7108.
(7) Nelsen, S. F.; Ismagilov, R. F. *J. Phys. Chem. A* **1999**, *103*, 5373.
(8) Nelsen, S. F.; Ramm, M. T.; Wolff, J. J.; Powell, D. R. *J. Am. Chem. Soc.* **1997**, *119*, 6863.
(9) Sun, D.-L.; Rosokha, S. V.; Lindeman, S. V.; Kochi, J. K. *J. Am. Chem. Soc.* **2003**, *125*, 15950.
(10) Lindeman, S. V.; Rosokha, S. V.; Sun, D.-L.; Kochi, J. K. *J. Am. Chem. Soc.* **2002**, *124*, 843.
(11) Lahlil, K.; Moradpour, A.; Bowlas, C.; Menou, F.; Cassoux, P.; Bonvoisin, J.; Launay, J.-P.; Dive, G.; Dehareng, D. *J. Am. Chem. Soc.* **1995**, *117*, 9995.
(12) Gautier, N.; Dumur, F.; Lloveras, V.; Vidal-Gancedo, J.; Veciana, J.; Rovira, C.; Hudhomme, P. *Angew. Chem., Int. Ed.* **2003**, *42*, 2765.
(13) Li, H.; Lambert, C. *Chem.—Eur. J.* **2006**, *12*, 1144.
(14) Bonvoisin, J.; Launay, J.-P.; Verbouwe, W.; Van der Auweraer, M.; De Schryver, F. C. *J. Phys. Chem. A* **1996**, *100*, 17079.
(15) Amthor, S.; Lambert, C. *J. Phys. Chem. A* **2006**, *110*, 1177.
(16) Barlow, S.; Risko, C.; Chung, S.-J.; Tucker, N. M.; Coropceanu, V.; Jones, S. C.; Levi, Z.; Brédas, J.-L.; Marder, S. R. *J. Am. Chem. Soc.* **2005**, *127*, 16900.
(17) Coropceanu, V.; Malagoli, M.; André, J. M.; Brédas, J.-L. *J. Chem. Phys.* **2001**, *115*, 10409.
(18) Coropceanu, V.; Malagoli, M.; André, J. M.; Brédas, J.-L. *J. Am. Chem. Soc.* **2002**, *124*, 10519.
(19) Coropceanu, V.; Lambert, C.; Nöll, G.; Brédas, J.-L. *Chem. Phys. Lett.* **2003**, *373*, 153.
(20) Coropceanu, V.; Gruhn, N. E.; Barlow, S.; Lambert, C.; Durivage, J. C.; Bill, T. G.; Nöll, G.; Marder, S. R.; Brédas, J.-L. *J. Am. Chem. Soc.* **2004**, *126*, 2727.
(21) Heckmann, A.; Amthor, S.; Lambert, C. *Chem. Commun.* **2006**, 2959.
(22) Hirao, Y.; Urabe, M.; Ito, A.; Tanaka, K. *Angew. Chem., Int. Ed.* **2007**, *46*, 3300.
(23) Jones, S. C.; Coropceanu, V.; Barlow, S.; Kinnibrugh, T.; Timofeeva, T.; Brédas, J.-L.; Marder, S. R. *J. Am. Chem. Soc.* **2004**, *126*, 11782.
(24) Lambert, C.; Nöll, G. *J. Am. Chem. Soc.* **1999**, *121*, 8434.

10.1021/ja9070859 CCC: $40.75

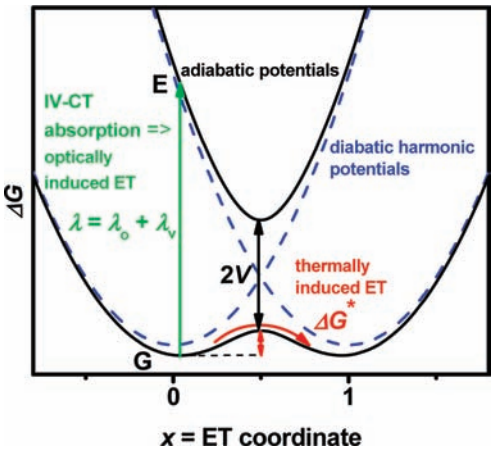

Figure 1. Adiabatic potential energy surfaces obtained by coupling two harmonic diabatic potentials along a single asymmetrical ET coordinate.

from a solvent contribution λ_o and a vibrational intramolecular contribution λ_v) and the electronic coupling V between the diabatic (formally noninteracting) states in which the charge is localized at one or the other redox center, respectively. In a one-dimensional harmonic approximation, the reorganization energy refers to the force constant of one diabatic potential.[4,29] If twice the electronic coupling is smaller than the reorganization energy, coupling of the two harmonic potentials results in a double minimum for the adiabatic ground-state potential surface and a single minimum for the excited-state potential. The energy splitting between the ground state and the excited state at the position of the transition state between the two minima then is exactly $2V$. However, if $2V > \lambda$, a single-minimum potential for the ground-state results. Those MV systems that fulfill $2V < \lambda$ are called Robin−Day class II systems, those with $2V > \lambda$ are called class III systems, according to the degree of electronic coupling. Thus, $2V < \lambda$ and $2V > \lambda$ represent two quite different situations. In the former, the MV compound is symmetry-broken (double minimum) and the charge can be transferred either optically or thermally from one redox center to the other: $M^+-B-M \rightarrow M-B-M^+$. In the latter case (single minimum) the MV system is symmetrical and the charge is symmetrically delocalized between both redox centers.

A central ongoing debate is how to discern the two situations mentioned before, class II and class III, experimentally.[29−32] Simple classical theory predicts for class II species a symmetrical Gaussian-shaped intervalence charge transfer (IV-CT) band in the near-infrared which is associated with the optically induced transfer of the charge from one redox center to the other. This band should be highly solvent-dependent as more polar solvents increase the λ_v contribution to λ which approximately refers to the optical excitation energy of the IV-CT band. In contrast, for class III species the IV-CT band should be highly asymmetrical (possibly with vibrational fine structure visible) and largely solvent-independent. However, in practice, particularly at the border between class II and class III it is often impossible to decide whether the charge in a MV compound is localized or delocalized. Thus, quantum chemical computations would be highly desirable to enable a computational Robin−Day classification as well as the quantitative prediction of various properties of the ground and excited states of such MV compounds. However, it has turned out that this is a challenge for the existing computational methodology.[18] Hartree−Fock (HF) theory, either within an *ab initio* or semiempirical MO framework, strongly overestimates charge localization and tends to provide localized MV structures even in cases where experimental evidence points clearly to a delocalized class III situation.[24,33] Structural symmetry breaking occurs, accompanied by substantial spin contamination, and unrealistically large dipole moments are predicted. Clearly, electron correlation has to be included for an adequate description. Unfortunately, accurate *ab initio* post-Hartree−Fock methods tend to be too involved and computationally expensive to be currently applied to structural optimizations for the size of MV compounds of chemical or technological interest. Semiempirical CI approaches like the AM1-CISD method may partly correct the situation,[26,34−38] but their predictive power is limited. Today, the most widely used methodology to incorporate electron correlation for larger systems (within a formally single-determinant approach) is Kohn−Sham density functional theory (DFT). However, DFT with "pure" (i.e., local or gradient corrected) or standard hybrid exchange-correlation functionals has been found to give an overly delocalized description.[18,19] That is, even localized class II systems are typically computed to be delocalized. This has to do with the self-interaction error (SIE) in the standard functionals, which favors too pronounced delocalization.

Delocalization artifacts due to SIE in DFT are well-known in many areas, from solid-state physics[39,40] via transition-metal ligand bonding[41] to organic π-systems.[42−47] The latter are most closely related to the organic MV systems we want to study here. Efforts to reduce the SIE in exchange-correlation functionals include so-called range-separated hybrid functionals,[48] local hybrid functionals with position-dependent exact-exchange

(25) Lambert, C.; Gaschler, W.; Schmälzlin, E.; Meerholz, K.; Bräuchle, C. *J. Chem. Soc., Perkin Trans. 2* **1999**, 577.
(26) Lambert, C.; Amthor, S.; Schelter, J. *J. Phys. Chem. A* **2004**, *108*, 6474.
(27) Utz, N.; Koslowski, T. *Chem. Phys.* **2002**, *282*, 389.
(28) Kattnig, D. R.; Mladenova, B.; Grampp, G.; Kaiser, C.; Heckmann, A.; Lambert, C. *J. Phys. Chem. C* **2009**, *113*, 2983.
(29) Brunschwig, B. S.; Creutz, C.; Sutin, N. *Chem. Soc. Rev.* **2002**, *31*, 168.
(30) Nelsen, S. F. *Chem.—Eur. J.* **2000**, *6*, 581.
(31) Demadis, K. D.; Hartshorn, C. M.; Meyer, T. J. *Chem. Rev.* **2001**, *101*, 2655.
(32) Nelsen, S. F.; Schultz, K. P.; Telo, J. P. *J. Phys. Chem. A* **2008**, *112*, 12622.
(33) Nelsen, S. F.; Blomgren, F. *J. Org. Chem.* **2001**, *66*, 6551.
(34) Heckmann, A.; Lambert, C.; Goebel, M.; Wortmann, R. *Angew. Chem., Int. Ed.* **2004**, *43*, 5851.
(35) Lambert, C.; Nöll, G. *Angew. Chem., Int. Ed.* **1998**, *37*, 2107.
(36) Lambert, C.; Nöll, G.; Hampel, F. *J. Phys. Chem. A* **2001**, *105*, 7751.
(37) Nelsen, S. F.; Reinhardt, L. A.; Tran, H. Q.; Clark, T.; Chen, G. F.; Pappas, R. S.; Williams, F. *Chem.—Eur. J.* **2002**, *8*, 1074.
(38) Nelsen, S. F.; Weaver, M. N.; Konradsson, A. E.; Telo, J. P.; Clark, T. *J. Am. Chem. Soc.* **2004**, *126*, 15431.
(39) Gerber, I. C.; Angyan, J. G.; Marsman, M.; Kresse, G. *J. Chem. Phys.* **2007**, *127*, 054101/1.
(40) Cora, F. *Mol. Phys.* **2005**, *103*, 2483.
(41) See, for example: Remenyi, C. R., R.; Kaupp, M. *J. Phys. Chem. B* **2007**, *111*, 8290. Kaupp, M.; Reviakine, R.; Malkina, O. L.; Arbuznikov, A.; Schimmelpfennig, B.; Malkin, V. G. *J. Comput. Chem.* **2002**, *23*, 794, and references therein.
(42) See, for example: Sancho-Garcia, J. C. *J. Chem. Phys.* **2006**, *124*, 124112.
(43) Sancho-Garcia, J. C.; Perez-Jimenez, A. J. *Phys. Chem. Chem. Phys.* **2007**, *9*, 5874.
(44) Sanchez-Carrera, R. S.; Coropceanu, V.; da Silva Filho, D. A.; Friedlein, R.; Osikowicz, W.; Murdey, R.; Suess, C.; Salaneck, W. R.; Brédas, J.-L. *J. Phys. Chem. B* **2006**, *110*, 18904.
(45) Zhao, Y.; Truhlar, D. G. *J. Phys. Chem. A* **2006**, *110*, 10478.
(46) Salzner, U.; Pickup, P. G.; Poirieri, R. A.; Lagowski, J. B. *J. Phys. Chem. A* **1998**, *102*, 2572.
(47) Dierksen, M.; Grimme, S. *J. Phys. Chem. A* **2004**, *108*, 10225.

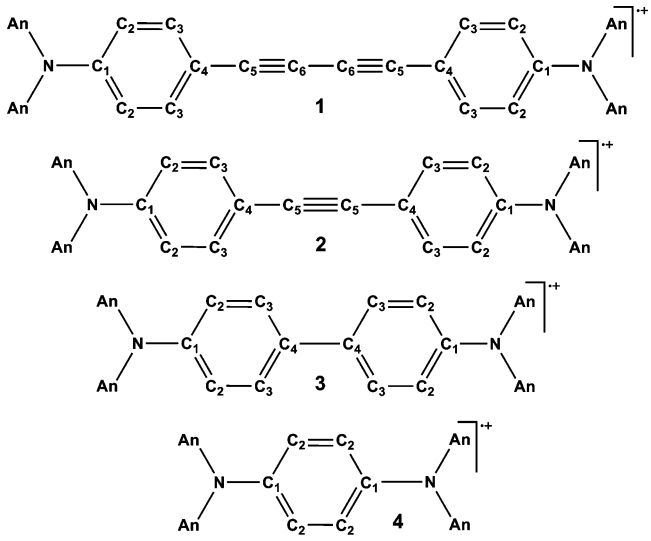

Figure 2. Four bistriarylamin radical cations investigated (An = 4-methoxyphenyl).

admixture,[49−51] and other approaches classified generally as hyper-GGA functionals.[52−55] In the specific field of organic MV compounds, extended studies of improved methodologies are lacking so far. The aim of the present work is to provide a basis for such investigations by examining the decisive aspects that control the outcome of DFT calculations on organic MV systems. For a systematic validation study, we have selected a series of four mixed-valence bistriarylamin radical cations (Figure 2) that are all close to the class II/III borderline, but to a different extent, and have been studied experimentally in detail (as well as by standard DFT and time-dependent DFT (TDDFT) calculations, albeit only for symmetrical ground-state structures without including solvent effects[18]). These cations differ exclusively in the bridge between the two triarylamine centers. The decreasing distance between the triarylamine redox centers in **1**−**4** goes along with an increase of electronic coupling between the associated diabatic states as obtained by analysis of the NIR spectra within a two-dimensional two-state model including an asymmetric as well as a symmetric ET coordinate[15] (in cm^{-1}): V = 1790 (**1**), 2400 (**2**), 2800 (**3**), and 4300 (**4**).

Our Strategy Will Be 3-Fold. (a) We will systematically vary the amount of exact-exchange admixture a in a set of general global hybrid functionals and will examine the value of a (see eq 1 below) at which vibronic charge localization occurs. This will be done by scrutinizing in each case structure, dipole-moment, spin-density distribution, and electron-transfer barrier. Larger a values will diminish SIE and enhance spin polarization. However, too large exact-exchange admixtures are expected to lead to artifacts arising from spin contamination, and from an incorrect description of nondynamical electron correlation effects.

(b) Most experiments on such systems are carried out in solution. Due to the inherent charge separation in the localized case, we expected that solvent effects will decisively influence the point of symmetry breaking. We will therefore compare in each case gas-phase results with computations including solvent effects via a conductor-like screening (COSMO[56]) continuum solvent model for the nonpolar solvent hexane, the polar solvent acetonitrile, and to some extent the intermediate-polarity solvent dichloromethane (which is predominantly used for Vis/NIR spectroscopy on these systems). This should enable us not only to quantify the influence of dielectric solvent effects on the charge localization/delocalization preferences in organic MV radical cations but should also provide us with guidelines for a practical computational protocol (see below).

(c) Only limited direct experimental data is available on ground-state structures: a few symmetrical structures have been characterized in the solid state, and the effect of crystal environment on symmetry breaking is being debated.[57] A host of information has been used so far to discuss the class II vs class III character (e.g., generalized Mulliken-Hush analysis of the IV-CT bands,[15,26] photoelectron spectroscopy,[20,58] IR and Raman vibrational spectroscopy,[59] and EPR-spectroscopy,[16,22,28,60] see below for further details). Here we will use in particular a comparison of IV-CT transition energies computed by TDDFT for localized and delocalized structures to characterize the nature of the system for a given solvent. We arrive at a computational protocol, based on hybrid functionals, continuum solvent models, and TDDFT computation of excitation energies, that allows a reliable positioning of such organic MV systems along the localized-delocalized coordinate. A basis is thus obtained to evaluate alternative, possibly more sophisticated methodologies in the future.

2. Available Experimental Information

The four organic mixed-valence radical cations studied (see Figure 2) all feature two *N,N*-di(4-methoxyphenyl)-moieties with different bridges. Compound **1**, (*bis*-{4-[*N,N*-di(4-methoxyphenyl)amino]phenyl}butadiyne, has the largest separation between the coupled redox centers. This distance is successively shortened by changing the bridge to a single diphenylacetylene in **2**, *bis*-acetylene, to a biphenylene bridge in **3**, 4,4′-*bis*[*N,N*-di(4-methoxyphenyl)amino]biphenyl, to a single phenylene bridge in **4**, *N,N,N′,N′*-tetra(4-methoxyphenyl)-1,4-phenylenediamine. Experimental evidence points to a class II character of **1**, albeit with substantial electronic coupling.[24] Compound **2** is more strongly coupled but was indicated to be possibly still just on the class II side, based on the shape of the IV-CT band and on the lack of inversion symmetry in the vibrational spectra in CH_2Cl_2 (on the EPR time scale, no symmetry breaking has been detected, which suggests a small electron-transfer barrier).[16,24,35] On the basis of NIR spectra and vibrational data,

(48) See, for example: Henderson, T. M.; Janesko, B. G.; Scuseria, G. E. *J. Phys. Chem. A* **2008**, *112*, 12530.
(49) Jaramillo, J.; Scuseria, G. E.; Ernzerhof, M. *J. Chem. Phys.* **2003**, *118*, 1068.
(50) Bahmann, H.; Rodenberg, A.; Arbuznikov, A. V.; Kaupp, M. *J. Chem. Phys.* **2007**, *126*, 011103/1.
(51) Perdew, J. P.; Staroverov, V. N.; Tao, J.; Scuseria, G. E. *Phys. Rev. A: At., Mol., Opt. Phys.* **2008**, *78*, 052513/1.
(52) Mori-Sanchez, P.; Cohen, A. J.; Yang, W. *J. Chem. Phys.* **2006**, *124*, 091102/1.
(53) Cohen, A. J.; Mori-Sanchez, P.; Yang, W. *J. Chem. Phys.* **2007**, *126*, 191109/1.
(54) Cohen, A. J.; Mori-Sanchez, P.; Yang, W. *J. Chem. Phys.* **2007**, *127*, 034101/1.
(55) Becke, A. D. *J. Chem. Phys.* **2005**, *122*, 064101/1.
(56) Klamt, A.; Schuurmann, G. *J. Chem. Soc., Perkin Trans. 2* **1993**, 799.
(57) Low, P. J.; Paterson, M. A. J.; Puschmann, H.; Goeta, A. E.; Howard, J. A. K.; Lambert, C.; Cherryman, J. C.; Tackley, D. R.; Leeming, S.; Brown, B. *Chem.—Eur. J.* **2004**, *10*, 83.
(58) Lambert, C.; Risko, C.; Coropceanu, V.; Schelter, J.; Amthor, S.; Gruhn, N. E.; Durivage, J. C.; Brédas, J.-L. *J. Am. Chem. Soc.* **2005**, *127*, 8508.
(59) Szeghalmi, A. V.; Erdmann, M.; Engel, V.; Schmitt, M.; Amthor, S.; Kriegisch, V.; Nöll, G.; Stahl, R.; Lambert, C.; Leusser, D.; Stalke, D.; Zabel, M. *J. Am. Chem. Soc.* **2004**, *126*, 7834.
(60) Lancaster, K.; Odom, S. A.; Jones, S. C.; Thayumanavan, S.; Marder, S. R.; Brédas, J.-L.; Coropceanu, V.; Barlow, S. *J. Am. Chem. Soc.* **2009**, *131*, 1717.

compound **3** is likely just on the class III side of the border,[57] whereas **4** should probably be considered a more clear-cut class III case (see also below).[59] X-ray structure determinations for salts of systems closely related to **3** and **4** (derivatives without the methoxy substituents) gave symmetrical structures which is also supported by Raman and IR spectroscopic measurements.[59]

3. Computational Details

Structure optimizations as well as bonding analyses were performed with a locally modified version of TURBOMOLE 5.9 and 5.10,[61] that allows the exact-exchange admixture in a global hybrid functional to be varied. The "custom hybrid" exchange-correlation functionals were constructed according to eq 1 by varying the exact-exchange coefficient a, largely in steps of 0.1, between 0.0 and 1.0, i.e. between the "pure" gradient-corrected BLYP functional[62,63] ($a = 0.0$) via the BHLYP hybrid functional with 50% exact exchange ($a = 0.5$) to a functional made from 100% exact exchange ($a = 1.0$) with LYP correlation[63] on top (we skip the point $a = 0.1$, as it brings little further information). In some cases, pure HF calculations without correlation functional have also been performed. SVP basis sets were employed on all atoms[64] (test calculations with larger TZVP basis sets did not change the obtained results noticeably).

$$E_{XC} = (1 - a)(E_X^{LSDA} + \Delta E_X^{B88}) + aE_X^{HF} + E_C^{LYP} \quad (1)$$

In addition to gas-phase optimizations, in all cases optimizations with the COSMO solvent model[56] have been used for hexane ($\varepsilon = 1.89$), for dichloromethane ($\varepsilon = 8.93$), and for acetonitrile ($\varepsilon = 36.64$). Near the critical values of a, where symmetry breaking occurs, the outcome of the structure optimizations depended sometimes on whether we used a symmetrical or unsymmetrical starting structure. In those cases, we therefore tried unsymmetrical starting structures (C_1) as well as symmetrical ones (C_i). For unsymmetrical cases, this led to a lower energy of the symmetry-broken structure. For **1**, different rotational conformers have been investigated. In some cases (for **1**, $a = 0.3$ in acetonitrile, $a = 0.4$ in the gas phase and in acetonitrile, $a = 0.6$ in hexane, and $a = 0.8$ in the gas phase and in acetonitrile), the stationary points on the potential energy surface have been characterized by harmonic vibrational frequency analysis. The electron transfer barrier was subsequently calculated as the energy difference between the C_i-symmetric transition state and the unsymmetric C_1-optimized minimum. Spin-density isosurface plots were obtained with the Molekel program.[65]

Subsequent TDDFT-calculations of the lowest-energy electronic transitions (IV-CT bands) for both C_1 and C_i structures were done with the Gaussian 03 program,[66] using the same type of custom hybrids and SVP basis sets[64] as discussed above. In the Gaussian 03 calculations, solvent effects have been included by the CPCM keyword, which denotes the polarizable continuum model that is closest to the COSMO model used in the optimizations.[67] However, calculations with the more sophisticated IEF-PCM model[68] gave almost identical data. The use of Gaussian 03 was initially motivated by the lack of a custom hybrid TDDFT implementation in our local version of Turbomole. During the course of this work, the custom hybrids were implemented, and test calculations with Turbomole were done. While gas-phase calculations gave almost identical results as the Gaussian 03 data, the solvent-based calculations gave about 150−500 cm^{-1} larger excitation energies (depending on functional and system) for clearly localized, unsymmetrical structures, and about 800−1800 cm^{-1} larger values for symmetrical structures. As the Gaussian 03 results were consistently much closer to experiment, they are reported here. Obviously, the differences arise from technical details (van-der-Waals radii, solvent radii, number of tesserae per sphere) in the two solvent-model implementations. It is ongoing work to elucidate which of these is mainly responsible, and to readjust parameters.

We note in passing that test calculations with hybrid functionals constructed from other gradient-corrected exchange and correlation contributions (PBE) gave slightly shorter bonds but essentially the same behavior regarding the fraction of exact exchange at which vibronic charge localization occurs in a given environment (and similar IV-CT excitation energies).

4. Results and Discussion

Ground-State Calculations. The main results for the ground states of the radical cations **1**−**4**, respectively, are summarized in Tables 1−4, which provide the C_{An}−N distances as indication for structural symmetry breaking (further structural data are available in Tables S1−S4 in Supporting Information), the dipole moments, the electron transfer barriers, as well as the S^2 expectation values. Comparison of the latter has to be taken with some caution for hybrid DFT computations with different amounts of nonlocal Hartree−Fock-like exchange but should provide a reasonable measure of the quality of the spin-density distributions obtained. Figure 3 gives an illuminating overview over the most important trends by plotting the computed electron transfer barriers for compounds **1**−**3** (**4** remains delocalized - class III - at all DFT levels in the gas phase and in all solvent models; see below).

Let us first examine the general trends before looking at the individual MV radical cations in more detail. Taking the exact-exchange admixture a at which symmetry breaking occurs and an ET barrier develops in a given environment (gas phase vs hexane vs dichloromethane vs acetonitrile solvent) as an indication for the localized vs delocalized character, the expected trend from **1** toward **4** is found: the critical exact-exchange admixture at which a barrier is formed in a given environment moves from left to right (compare Tables 1−4 and Figure 3), consistent with the weakest electronic coupling for the longest bridge in **1** and with the strongest coupling for the shortest bridge in **4**.

The influence of the COSMO continuum solvent is striking. All gas-phase calculations require exceedingly large exact-exchange admixtures for symmetry breaking even for compound **1**, which should be most clearly on the localized class II side. A low-polarity solvent like hexane moves the point of symmetry breaking to a somewhat lower value of a. Yet, the effect of the more polar dichloromethane and acetonitrile solvents is much larger, indicating that solvent polarity may have a dramatic effect on the electron-transfer characteristics of a given MV radical

(61) Ahlrichs, R.; Bär, M.; Häser, M.; Horn, H.; Köhmel, C. *Chem. Phys. Lett.* **1989**, *162*, 165.
(62) Becke, A. D. *Phys. Rev. A* **1988**, *38*, 3098.
(63) Lee, C.; Yang, W.; Parr, R. G. *Phys. Rev. B: Condens. Matter* **1988**, *37*, 785.
(64) Schäfer, A.; Horn, H.; Ahlrichs, R. *J. Chem. Phys.* **1992**, *97*, 2571.
(65) Portmann, S.; Luthi, H. P. *Chimia* **2000**, *54*, 766.
(66) Frisch, M. J.; et al. *Gaussian 03*, revision E.01; Gaussian, Inc.: Wallingford, CT, 2004.
(67) Barone, V.; Cossi, M. *J. Phys. Chem. A* **1998**, *102*, 1995.
(68) Cancès, E.; Menucci, B. *J. Chem. Phys.* **2001**, *114*, 4744.

Table 1. Calculated Key Ground-State Parameters for **1** As a Function of Exact-Exchange Admixture and Solvent Environment

%HF	BLYP	20	30	35	40	50	60	70	80	90	100
					gas phase						
μ [D]	0.02	0.14	0.01	0.03	0.03	0.03	0.04	22.09	25.38	27.30	28.37
ΔG^* ($C_i - C_1$) [kJ/mol]	0.00	−0.01	−0.03	0.02	0.00	−0.01	−0.01	1.90	8.09	16.83	27.37
$\langle S^2 \rangle$	0.75	0.76	0.77	0.78	0.78	0.80	0.81	0.94	1.05	1.23	1.49
C_{An}−N [Å]	1.436	1.429	1.427	1.426	1.425	1.425	1.423	1.418	1.413	1.409	1.406
	1.436	1.429	1.427	1.426	1.425	1.425	1.423	1.407	1.400	1.394	1.391
					hexane						
μ [D]	0.05	0.39	0.02	0.02	0.06	19.34	26.42	28.24	29.13	29.91	30.21
ΔG^* ($C_i - C_1$) [kJ/mol]	0.04	−0.03	0.00	0.03	0.03	0.16	4.72	11.19	18.92	27.96	39.35
$\langle S^2 \rangle$	0.75	0.76	0.77	0.78	0.78	0.82	0.88	0.95	1.06	1.23	1.49
C_{An}−N [Å]	1.436	1.429	1.427	1.426	1.426	1.412	1.401	1.397	1.393	1.389	1.387
	1.436	1.430	1.427	1.426	1.425	1.424	1.420	1.416	1.412	1.409	1.406
					dichloromethane						
μ [D]	0.02	0.39	5.03	26.82	29.33	31.24	31.89	32.17	32.23	32.22	32.32
ΔG^* ($C_i - C_1$) [kJ/mol]	0.31	0.19	0.15	3.20	6.08	13.27	20.90	28.46	36.90	45.90	57.48
$\langle S^2 \rangle$	0.75	0.76	0.77	0.79	0.80	0.82	0.87	0.94	1.05	1.23	1.50
C_{An}−N [Å]	1.435	1.428	1.424	1.408	1.404	1.422	1.393	1.429	1.412	1.409	1.405
	1.435	1.428	1.428	1.428	1.426	1.398	1.419	1.426	1.389	1.386	1.385
					acetonitrile						
μ [D]	0.04	3.56	28.07	29.89	31.17	32.27	32.75	33.14	33.13	33.04	32.97
ΔG^* ($C_i - C_1$) [kJ/mol]	0.45	0.56	3.65	7.21	10.78	18.57	25.92	33.61	41.58	51.29	62.76
$\langle S^2 \rangle$	0.75	0.76	0.78	0.79	0.80	0.82	0.87	0.93	1.04	1.22	1.49
C_{An}−N [Å]	1.435	1.427	1.409	1.406	1.402	1.397	1.393	1.388	1.386	1.384	1.382
	1.435	1.430	1.430	1.428	1.426	1.422	1.419	1.415	1.412	1.409	1.406

Table 2. Calculated Key Ground-State Parameters for **2** As a Function of Exact-Exchange Admixture and Solvent Environment

%HF	BLYP	20	30	35	40	50	60	70	80	90	100
					gas phase						
μ [D]	0.02	0.14	0.09	0.03	0.04	0.01	0.12	0.18	13.92	17.52	21.40
ΔG^* ($C_i - C_1$) [kJ/mol]	−0.01	−0.02	−0.01	−0.01	−0.03	−0.03	0.01	0.05	0.43	4.31	11.84
$\langle S^2 \rangle$	0.75	0.76	0.77	0.77	0.78	0.79	0.80	0.82	0.93	1.07	1.36
C_{An}−N [Å]	1.435	1.429	1.427	1.426	1.426	1.424	1.423	1.421	1.416	1.412	1.407
	1.435	1.429	1.426	1.425	1.426	1.425	1.423	1.421	1.412	1.407	1.393
					hexane						
μ [D]	0.04	0.10	0.08	1.25	0.18	0.02	0.16	18.33	20.58	23.04	23.98
ΔG^* ($C_i - C_1$) [kJ/mol]	0.00	0.06	0.05	−0.15	0.03	0.02	0.08	1.76	5.69	12.30	20.39
$\langle S^2 \rangle$	0.75	0.76	0.77	0.77	0.78	0.79	0.80	0.91	1.01	1.17	1.41
C_{An}−N [Å]	1.435	1.428	1.427	1.428	1.426	1.425	1.423	1.419	1.416	1.410	1.405
	1.435	1.428	1.427	1.425	1.426	1.425	1.423	1.407	1.401	1.392	1.389
					dichloromethane						
μ [D]	0.02	0.10	0.07	10.07	19.83	23.14	25.17	25.82	25.76	25.74	26.06
ΔG^* ($C_i - C_1$) [kJ/mol]	0.10	0.07	0.09	0.11	0.74	4.35	8.54	13.17	18.44	24.94	33.29
$\langle S^2 \rangle$	0.75	0.76	0.77	0.78	0.79	0.82	0.86	0.93	1.03	1.18	1.42
C_{An}−N [Å]	1.435	1.428	1.427	1.428	1.427	1.427	1.426	1.427	1.413	1.410	1.406
	1.435	1.428	1.426	1.421	1.410	1.427	1.427	1.426	1.389	1.387	1.385
					acetonitrile						
μ [D]	0.03	1.39	0.27	20.09	23.30	25.48	26.22	26.35	26.67	26.73	26.84
ΔG^* ($C_i - C_1$) [kJ/mol]	0.12	0.15	0.18	1.54	3.40	7.54	12.01	17.02	22.20	28.56	37.07
$\langle S^2 \rangle$	0.75	0.76	0.77	0.78	0.79	0.82	0.86	0.93	1.03	1.19	1.43
C_{An}−N [Å]	1.435	1.428	1.427	1.428	1.426	1.422	1.418	1.416	1.412	1.408	1.405
	1.435	1.429	1.427	1.412	1.406	1.399	1.394	1.392	1.388	1.387	1.384

cation[69,70] (in dichloromethane, the point of symmetry breaking is at about 5−10%age points larger than in acetonitrile). Electrochemical and spectroscopic experiments on such radical ions are usually done in such solvents of moderate to appreciable polarity. We therefore regard the acetonitrile results as a reasonably realistic simulation of typical experimental conditions for electrochemistry, and the dichloromethane results as particularly realistic for optical spectroscopy (see below).

Now we look more closely at the results for the individual cations. For the most clear-cut class II case **1**, gas-phase calculations require about 70% exact-exchange admixture for symmetry breaking (Table 1, Figure 3). This is accompanied by substantial spin contamination, which indicates unphysically large valence-shell spin polarization. A COSMO hexane model shifts the critical *a* value from 0.7 to 0.6, still with substantial spin contamination in the localized case (Table 1). Notably, both in the gas phase and in hexane, the critical step in *a* from a delocalized to a localized solution is accompanied by a dramatic enhancement of the S^2 expectation value. In contrast, in acetonitrile, charge localization starts to occur at more reasonable

(69) Nelsen, S. F.; Trieber, D. A.; Ismagilov, R. F.; Teki, Y. *J. Am. Chem. Soc.* **2001**, *123*, 5684.
(70) Nelsen, S. F.; Weaver, M. N.; Telo, J. P. *J. Am. Chem. Soc.* **2007**, *129*, 7036.

Table 3. Calculated Key Ground-State Parameters for **3** As a Function of Exact-Exchange Admixture and Solvent Environment

%HF	BLYP	20	30	35	40	50	60	70	80	90	100
					gas phase						
μ [D]	0.02	0.10	0.02	0.03	0.19	0.04	0.04	0.02	0.05	12.73	15.45
ΔG^* ($C_i - C_1$) [kJ/mol]	0.00	−0.02	−0.02	−0.01	−0.31	0.04	−0.01	0.00	−0.02	0.71	5.34
$\langle S^2 \rangle$	0.75	0.76	0.77	0.77	0.78	0.79	0.80	0.81	0.83	1.04	1.28
C_{An}−N [Å]	1.434	1.427	1.426	1.425	1.424	1.424	1.422	1.420	1.418	1.412	1.407
	1.434	1.428	1.426	1.425	1.425	1.424	1.422	1.420	1.418	1.405	1.397
					hexane						
μ [D]	0.01	0.19	0.04	0.03	0.02	0.09	0.06	0.02	9.20	12.18	16.85
ΔG^* ($C_i - C_1$) [kJ/mol]	0.00	0.04	0.10	0.08	0.15	0.07	0.08	0.08	0.54	2.79	8.87
$\langle S^2 \rangle$	0.75	0.76	0.77	0.77	0.78	0.79	0.80	0.81	0.89	1.01	1.34
C_{An}−N [Å]	1.434	1.427	1.426	1.426	1.425	1.424	1.422	1.420	1.416	1.412	1.406
	1.434	1.428	1.426	1.426	1.425	1.424	1.423	1.420	1.414	1.411	1.396
					dichloromethane						
μ [D]	0.01	0.36	0.27	0.05	0.17	0.12	18.19	18.33	18.88	19.66	19.87
ΔG^* ($C_i - C_1$) [kJ/mol]	0.19	0.23	0.27	0.29	0.80	0.74	2.08	4.39	7.01	11.61	17.84
$\langle S^2 \rangle$	0.75	0.76	0.77	0.77	0.78	0.79	0.85	0.91	1.00	1.15	1.38
C_{An}−N [Å]	1.434	1.427	1.426	1.426	1.425	1.425	1.420	1.416	1.412	1.409	1.405
	1.434	1.428	1.426	1.426	1.425	1.425	1.401	1.399	1.396	1.391	1.390
					acetonitrile						
μ [D]	0.05	0.80	0.08	6.34	13.28	18.07	19.16	19.69	20.02	19.94	20.25
ΔG^* ($C_i - C_1$) [kJ/mol]	0.33	0.30	0.42	0.39	0.72	2.27	4.41	6.99	9.39	11.78	18.85
$\langle S^2 \rangle$	0.75	0.76	0.77	0.77	0.79	0.81	0.85	0.91	1.00	1.19	1.42
C_{An}−N [Å]	1.434	1.428	1.427	1.427	1.426	1.423	1.419	1.416	1.412	1.407	1.404
	1.434	1.429	1.427	1.421	1.414	1.405	1.400	1.396	1.393	1.393	1.389

Table 4. Calculated Key Ground-State Parameters for **4** as a Function of Exact-Exchange Admixture and Solvent Environment. Further Results for $a = 0.7$ and $a = 0.9$ are Available in Table S4

%HF	BLYP	20	30	35	40	50	60	80	100	pure HF
					gas phase					
μ [D]	0.03	0.02	0.06	0.03	0.16	0.01	0.04	0.04	0.09	8.43
ΔG^* ($C_i - C_1$) [kJ/mol]	−0.02	0.00	−0.03	−0.02	−0.01	0.03	0.04	0.03	0.01	6.95
$\langle S^2 \rangle$	0.75	0.76	0.77	0.77	0.78	0.79	0.80	0.83	0.93	2.84
C_{An}−N [Å]	1.436	1.428	1.426	1.425	1.425	1.422	1.420	1.416	1.411	1.429
	1.435	1.428	1.426	1.425	1.424	1.422	1.420	1.416	1.412	1.414
					hexane					
μ [D]	0.01	0.01	0.02	0.03	0.04	0.01	0.03	0.01	0.08	9.47
ΔG^* ($C_i - C_1$) [kJ/mol]	0.06	0.04	0.10	0.03	0.02	0.11	−0.03	0.11	0.08	9.52
$\langle S^2 \rangle$	0.75	0.76	0.77	0.77	0.78	0.78	0.79	0.82	0.92	2.90
C_{An}−N [Å]	1.434	1.428	1.426	1.425	1.424	1.422	1.422	1.417	1.411	1.428
	1.435	1.428	1.426	1.425	1.424	1.423	1.422	1.417	1.411	1.412
					dichloromethane					
μ [D]	0.04	0.02	0.13	0.03	0.33	0.08	0.09	0.05	0.06	11.07
ΔG^* ($C_i - C_1$) [kJ/mol]	0.35	0.22	0.18	0.24	0.08	0.24	0.19	0.45	0.72	14.28
$\langle S^2 \rangle$	0.75	0.76	0.77	0.77	0.77	0.78	0.79	0.82	0.92	2.99
C_{An}−N [Å]	1.435	1.428	1.427	1.425	1.425	1.422	1.421	1.416	1.411	1.424
	1.435	1.428	1.426	1.425	1.423	1.422	1.420	1.416	1.411	1.409
					acetonitrile					
μ [D]	0.01	0.23	0.01	0.01	0.02	0.06	0.01	0.03	0.01	11.44
ΔG^* ($C_i - C_1$) [kJ/mol]	0.44	0.38	0.40	0.41	0.46	0.46	0.52	0.75	1.02	15.47
$\langle S^2 \rangle$	0.75	0.76	0.77	0.77	0.77	0.78	0.79	0.82	0.90	3.00
C_{An}−N [Å]	1.435	1.429	1.426	1.426	1.424	1.423	1.421	1.417	1.412	1.424
	1.435	1.428	1.426	1.426	1.424	1.423	1.421	1.417	1.412	1.408

exact-exchange admixtures of about 30%. In this case, the S^2 value increases only very little, from 0.76 at $a = 0.2$ to 0.78 to $a = 0.3$, indicating almost negligible spin contamination. A further moderate increase is found at $a = 0.4$ and $a = 0.5$ in this case. The electron-transfer barrier increases also in a continuous fashion in acetonitrile, whereas the changes are more abrupt at the high a values needed in the gas phase or in hexane. The dichloromethane data indicate a slightly larger critical step at around 35% exact exchange.

Further confirmation for these conclusions comes from inspection of spin-density distributions (Figure 4): at 30% HF-like exchange in the gas phase (left), a perfectly symmetrical distribution with little spin polarization is seen. With the same exact-exchange admixture in acetonitrile, symmetry breaking occurs, and spin polarization becomes notable. The latter is largely restricted to the spin-carrying, oxidized half of the system. The situation at 70% HF-like exchange in the gas phase looks substantially different: here the spin polarization is dramatic, consistent with the large spin contamination (cf. Table 1), and it extends also to the nonoxidized part of the system (see Figure 4). We find similar behavior also for spin-density distributions of unsymmetrical **2** and **3** in the gas phase or in hexane at large exact-exchange admixtures (not shown). Investigations of other rotational conformers give very similar results.

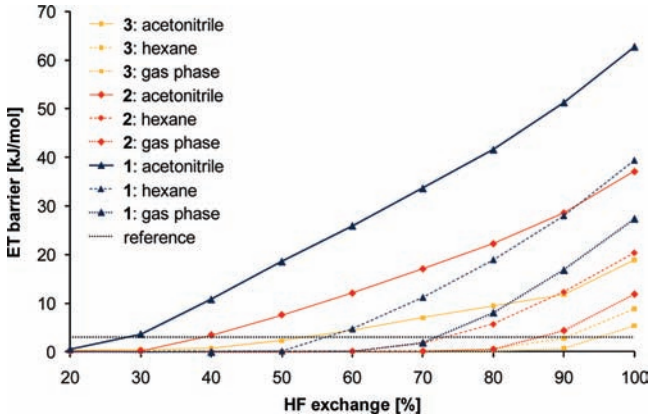

Figure 3. Electron-transfer barriers of **1**−**3** as a function of exact-exchange admixture and solvent environment. For **4** all functionals provide a zero barrier (Table 4). A reference line for small ET-barriers has arbitrarily been set at 3.0 kJ/mol.

Energy differences between the three conformers found (*P,P* and its enantiomer *M,M* as well as the meso compound *P,M*, all identified as minima on the potential energy surface) are below 1 kJ/mol, whereas dipole moments may differ by up to 4 D, depending on the arrangement of the methoxy groups.

On one hand these results make us confident that the symmetry breaking in acetonitrile solvent is not an artifact of an unsuitable functional, in contrast to the gas-phase or hexane calculations with large exact-exchange admixtures. On the other hand, at this point the acetonitrile and dichloromethane results provide us only with limited bracketing of the preferred *a* value, as we have no quantitative experimental data on the electron-transfer barrier, the structural symmetry breaking or the dipole moment. So far, a HF-like exchange admixture around 35% looks reasonable, but we cannot exclude 20 or 40%. At least we see already that a proper DFT description of the Robin−Day character of such systems may not be elusive.

We note in passing, that after the point of symmetry breaking the curves of the electron transfer barriers for the three cations **1**−**3** increase slightly more than linearly with exact-exchange admixture (Figure 3). Dipole moments show a dramatic increase around the critical *a* values and a rather moderate one to the right of it (Tables 1−3).

The classification of **4** is most straightforward (Table 4): in none of the four environments and at no value of *a*, symmetry-broken structures are obtained. There can thus be no doubt from the computational point of view that **4** is a class III system under all conceivable conditions. We have used this fact to evaluate the performance of pure HF calculations (Table 4): at HF level without a correlation functional added, unsymmetrical solutions are indeed obtained even in the gas-phase calculations when starting from an unsymmetrical structure. This is consistent with semiempirical MO results, which also give unphysical symmetry breaking for such class III cases[1,2] (see also ref 18 for an *ab initio* HF calculation).

TDDFT Excited-State Calculations. Tables 5−8 provide TDDFT results for the IV-CT excitation energies of **1**−**4**, respectively (a wider variety of results for more levels of structure optimization and for further excitations are given in Tables S5−S8 in Supporting Information). Data are given in each case for full optimizations without symmetry (C_1) and for symmetrical C_i structures. In localized cases, the former are minima and the latter the transition states for electron transfer. In delocalized situations, the C_1 optimizations should give identical structures as the C_i optimizations. As discussed above, this is not fully the case due to numerical limitations, and thus for completeness both sets of data are given in such cases. For **1**, Table 5 gives only data for one level of structure optimization (at 35% exact-exchange admixture; as optical spectroscopy has been done in dichloromethane, this is the preferred solvent here), but with different exact-exchange admixtures and solvent polarities in the TDDFT calculations (with 35% HF-like exchange we provide also gas-phase TDDFT results to quantify the total solvent shifts). As **2** is still delocalized at 35% HF-like exchange in dichloromethane, here we also include data at 40% exact exchange in the structure optimization (cf. Table 2), as this allows the comparison of a localized minimum and a delocalized transition state (Table 6). As symmetry breaking is difficult to achieve at moderate exact-exchange admixture for **3** in dichloromethane, in this case data for structures obtained at 50% HF-like exchange in acetonitrile have been included to evaluate the effect of symmetry breaking on the excitation energies (Table 7). Only for **4**, we get a delocalized structure at all levels and focus again on the structure obtained with 35% HF-like exchange in dichloromethane (Table 8).

Indeed, as a clear-cut class III case compound **4** is ideally suited to validate first the quality of the TDDFT calculations at the different levels, as no structural ambiguities arise here. We note, first of all, that solvent shifts of the IV-CT excitation frequency are small, amounting only to a few hundred cm^{-1} for this symmetrical system (cf. gas-phase and solvent data at 35% HF-like exchange in Table 8). The effect of changing exact-exchange admixture *a* is similarly small. Selecting the value for 35% HF-like exchange in dichloromethane, we overestimate the experimental value of 9530 cm^{-1} (this is the experimental absorption maximum in dichloromethane) by 615 cm^{-1} or by about 6%. This may be within systematic errors of about 5−10% arising from ion pairing effects that might be present in the experiments, but which have been neglected in the computations. The result suggests that the exact-exchange admixture of about 35%, which we found to be particularly suitable to describe the symmetry breaking in some of these MV radical cations (see above), may also be used to properly compute the IV-CT excitation energy.

With these results for the class III system **4** in mind, we may now turn to **1**, which we found to be on the class II side based on ground-state properties (see above). Here we have to compare the excitations at the localized C_1 minima and at the C_i-symmetrical transition states (Table 5). First of all we note again a relatively small dependence of the excitation frequency on solvent and exact-exchange admixture for the symmetrical structure, consistent with the results for **4** (yet total solvent shifts relative to the gas-phase result are larger than for **4**). Much larger blue shifts with increasing solvent polarity are found for the localized MV structure. This is the expected behavior for a charge-localized system. Now the dependence on exact-exchange admixture is also much more pronounced. For consistency, and based on the results for **4**, we will in the following regard the results with $a = 0.35$ (35% HF-like exchange) in dichloromethane as our reference point. The 6800 cm^{-1} obtained at this level for the localized C_1 minimum of **1** is only about 750 cm^{-1} (about 10%) below the experimental value. In contrast, a much lower excitation energy of 4230 cm^{-1} is obtained for the C_i transition state. This is completely consistent with the scheme for a localized class II system (cf. Figure 1), where the excitation at the localized minimum

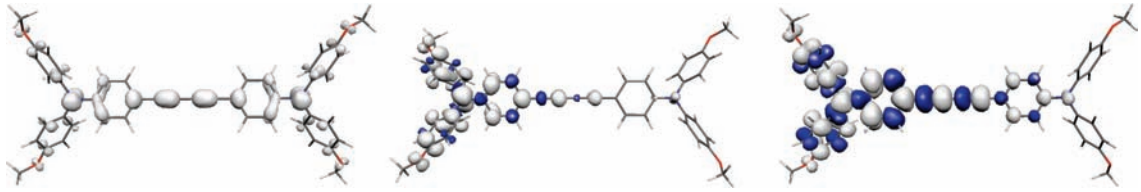

Figure 4. Spin-density isosurface plots (± 0.002 au) for **1**. Left, gas phase, $a = 0.3$; middle, acetonitrile, $a = 0.3$; right, gas phase, $a = 0.7$.

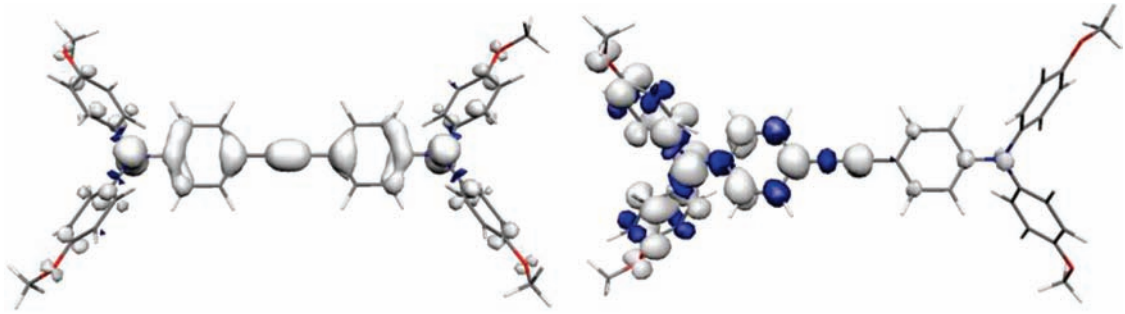

Figure 5. Spin-density isosurface plots (± 0.002 au) for **2**. Left, gas phase, $a = 0.4$; right, acetonitrile, $a = 0.4$.

Table 5. TDDFT Results for IV-CT Excitation Energies, E_1, and Transition Dipole Moments, μ_t, for **1** as Function of Exact-Exchange Admixture and Solvent[a]

			C_1 stucture		C_i structure	
ground-state structure	% HF for TDDFT	solvent for TDDFT	E_1 [cm^{-1}][b] (λ)	μ_t [D][c]	E_1 [cm^{-1}][d] ($2V$)	μ_t [D][c]
35% HF in dichloromethane						
	30	dichloromethane	5668	16.31	4655	24.45
		acetonitrile	6511	14.27	4843	23.77
	35	gas phase	4962	20.96	5865	20.85
		dichloromethane	**6800**	14.39	**4230**	26.30
		acetonitrile	7752	12.83	4451	25.43
	40	dichloromethane	8134	12.98	3646	29.03
		acetonitrile	9112	11.83	3920	27.79

[a] Boldface numbers are plotted in Figure 6. [b] The experimental value for λ (absorption maximum) in dichloromethane is 7550 cm^{-1}.[24] [c] Experimental transition moment μ_t in dichloromethane is 6.39 D.[24] [d] The experimental estimate for $2V$ from near-IR spectra[15] in dichloromethane is 3580 cm^{-1}.

Table 6. TDDFT Results for IV-CT Excitation Energies, E_1, and Transition Dipole Moments, μ_t, for **2** as Function of Exact-Exchange Admixture and Solvent[a]

			C_1 stucture		C_i structure	
ground-state structure	% HF for TDDFT	solvent for TDDFT	E_1 [cm^{-1}][b] (λ)	μ_t [D][c]	E_1 [cm^{-1}][d] ($2V$)	μ_t [D][c]
35% HF in dichloromethane						
	30	dichloromethane	5693	19.84	5653	20.56
		acetonitrile	6048	18.84	5862	20.04
	35	gas phase	6440	18.18	6646	18.09
		dichloromethane	**5745**	19.86	**5356**	21.61
		acetonitrile	6310	18.41	5593	20.99
	40	dichloromethane	6137	19.13	4972	22.94
		acetonitrile	6925	17.42	5247	22.18
40% HF in dichloromethane						
	30	dichloromethane	5955	17.40	5807	20.33
		acetonitrile	6521	15.98	6014	19.83
	35	gas phase	5979	18.17	6791	17.92
		dichloromethane	6561	16.31	5530	21.31
		acetonitrile	7289	14.89	5764	20.72
	40	dichloromethane	7460	15.10	5171	22.54
		acetonitrile	8278	13.85	5440	21.82

[a] Boldface numbers are plotted in Figure 6. [b] The experimental value for λ (absorption maximum) is 6190 cm^{-1} in dichloromethane[24] and 7990 cm^{-1} in acetonitrile.[35] [c] Experimental transition moment μ_t in dichloromethane is 11.6 D.[24] [d] The experimental estimate for $2V$ from near-IR spectra[15] in dichloromethane is 4800 cm^{-1}.

corresponds to the reorganization energy λ and the excitation energy at the symmetrical transition state corresponds to $2V$, i.e. two times the electronic coupling matrix element. As $\lambda > 2V$ for a class II system, the TDDFT results for **1** agree nicely with the class II character inferred from the ground-state calculations (see above).

We note in passing, that the transition dipole moment is in all cases appreciable (larger for symmetrical, delocalized

Table 7. TDDFT Results for IV-CT Excitation Energies, E_1, and Transition Dipole Moments, μ_t, for **3** as Function of Exact-Exchange Admixture and Solvent[a]

			C_1 stucture		C_i structure	
ground-state structure	% HF for TDDFT	solvent for TDDFT	E_1 [cm^{-1}][b] (λ)	μ_t [D][c]	E_1 [cm^{-1}][d] ($2V$)	μ_t [D][c]
35% HF in dichloromethane						
	30	dichloromethane	6843	16.87	6760	16.92
		acetonitrile	7065	16.47	6987	16.51
	35	gas phase	7544	17.48	7469	15.26
		dichloromethane	**6653**	17.48	**6561**	17.55
		acetonitrile	6898	17.03	6811	17.09
	40	dichloromethane	6405	18.19	6299	18.29
		acetonitrile	6678	17.68	6579	17.76
50% HF in acetonitrile						
	30	dichloromethane	6790	14.57	7642	15.88
		acetonitrile	7264	13.73	7866	15.52
	35	gas phase	6583	14.99	8272	14.45
		dichloromethane	7294	13.99	7541	16.33
		acetonitrile	7881	13.12	7785	15.94
	40	dichloromethane	8033	13.28	7392	16.86
		acetonitrile	8699	12.47	7658	16.42

[a] Boldface numbers are plotted in Figure 6. [b] The experimental value for λ (absorption maximum) in dichloromethane is 6360 cm^{-1}.[24] [c] Experimental transition moment μ_t in dichloromethane is 11.6 D.[24] [d] The experimental estimate for $2V$ from near-IR spectra[15] in dichloromethane is 5600 cm^{-1}.

Table 8. TDDFT Results for IV-CT Excitation Energies, E_1, and Transition Dipole Moments, μ_t, for **4** as Function of Exact-Exchange Admixture and Solvent[a]

			C_1 stucture		C_i structure	
ground-state structure	% HF for TDDFT	solvent for TDDFT	E_1 [cm^{-1}][b] (λ)	μ_t [D][c]	E_1 [cm^{-1}][d] ($2V$)	μ_t [D][c]
35% HF in dichloromethane						
	0	dichloromethane	9838	8.78	9819	8.75
	20	dichloromethane	9950	11.03	9906	11.01
		acetonitrile	10125	10.83	10080	10.81
	30	dichloromethane	10113	11.36	10054	11.35
		acetonitrile	10305	11.15	10244	11.14
	35	gas phase	10580	10.43	10526	10.41
		dichloromethane	**10145**	11.55	**10078**	11.54
		acetonitrile	10345	11.33	10277	11.33
	40	dichloromethane	10136	11.76	10060	11.75
		acetonitrile	10345	11.53	10269	11.53

[a] Boldface numbers are plotted in Figure 6. [b] The experimental value for λ (absorption maximum) in dichloromethane is 9530 cm^{-1}.[24] [c] Experimental transition moment μ_t in dichloromethane is 9.17 D.[24] [d] The experimental estimate for $2V$ from near-IR spectra[15] in dichloromethane is 8600 cm^{-1}.

structures but still notable for localized ones, Tables 5−8). We do therefore not expect systematic difficulties with TDDFT regarding too low transition energies[71] for small overlap between ground and excited state. This holds for delocalized as well as localized structures. Notably, from an orbital point of view the principal nature of the IV-CT transition does not change when going from the delocalized to the localized case: in general, the IV-CT band is dominated by the HOMO−LUMO transition. Compared to the experimental transition dipole moments the computed values are too large for **1**−**3** but agree well for **4** (cf. footnotes to Tables 5−8). For symmetrical structures we get the same trend as previous gas-phase TDDFT-B3LYP calculations (Table 2 in ref 18), but with slightly larger absolute values due to the inclusion of solvent effects (cf. also gas-phase data in Tables 5−8).

With this we turn to the true borderline case **2** (Table 6). Here the optimizations at 35% HF-like exchange in dichloromethane afforded a structure just on the verge of symmetry breaking, whereas the same DFT level gave clear symmetry breaking in acetonitrile. That is, we seem to be so close to the class II/III border that even this moderate increase of solvent polarity may determine the character observed. From the ground-state data alone, a clear classification remains thus elusive. To be able to discuss results for a clearly symmetry-broken structure, Table 6 includes also data obtained at structures optimized with $a = 0.4$ (in dichloromethane, cf. Table 2). For the C_1 minimum in the latter case, we do see a substantial dependence of the excitation energy on solvent and exact-exchange admixture as expected for a charge-localized state. In contrast, the excitation energies at the C_i transition state (and at the symmetrical structure obtained upon optimization at 35% exact-exchange admixture) exhibit again little dependence on solvent or functional. Based on the excitation energies computed in dichloromethane alone, no clear-cut answer is obtained for **2**. At $a = 0.35$, a localized structure gives an excitation energy about 6% *above* experiment, and a delocalized structure provides excitation energies about 10% *below* the experimental absorption maximum. This does not allow us to clearly classify **2** as localized or delocalized. However, for **2** an IV-CT frequency in acetonitrile is also available[35] (footnote b to Table 6), and it is clearly blue-shifted (by 1800 cm^{-1}) compared to the dichloromethane result. This is more in line with a localized ground state. The computationally predicted blue shift for a symmetrical structure is only about 200 cm^{-1}, that for a localized structure up to about 800 cm^{-1}, depending on structure and functional used (Table 6). While this is still too small relative to the

(71) See, for example: Dreuw, A.; Head-Gordon, M. *Chem. Rev.* **2005**, *105*, 4009.

experimental shift (where ion-pairing effects may enhance charge localization and thus the blue shifts), the solvent dependence points clearly to a class II character for **2**.

Finally, we move on to **3**, which based on the ground-state calculations should be more on the class III side than **2** (see above). In this case, the optimizations in dichloromethane at 35% HF-like exchange gave clearly a delocalized structure (cf. Table 3), and much larger exact-exchange admixtures are needed to force localization. Thus, Table 7 includes in addition to results for the structure with 35% in dichloromethane also those for the structure optimized at 50% in acetonitrile, providing charge localization (cf. Table 3). Here the excitation energies obtained with 35% HF-like exchange in dichloromethane differ relatively little between C_1 and C_i structures. They are larger for the structure obtained with 50% HF-like exchange in acetonitrile than for that computed with 35% HF-like exchange in dichloromethane, probably reflecting the overall somewhat shorter bonds at the former level (cf. Supporting Information, Tables S3 and S7). The results for the latter structure agree better with experiment. This alone does not allow a clear computational Robin-Day classification. However, together with the fact that rather large exact-exchange admixtures are needed to provoke symmetry breaking of the ground-state structure (Table 3) even in acetonitrile and even more so in dichloromethane, we feel that **3** may be assigned to the class III side, albeit close to the border.

A graphical summary of the computed IV-CT excitation energies (with structure optimizations as well as TDDFT calculations using 35% HF-like exchange in dichloromethane) in comparison with experiment is shown in Figure 6. In the case of **3** and **4**, differences between results obtained with C_1 and C_i structures, respectively, reflect only slight numerical inaccuracies in the optimizations and have no diagnostic meaning. As shown above, these two systems should be regarded as class III (although **3** is close to the borderline). Incidentally, in both cases, the C_i results are indeed very slightly closer to experiment. For **1** the much larger excitation energy computed for the localized C_1 structure agrees significantly better with experiment than the C_i result, consistent with the class II character found. For **2**, the C_1 structure at this computational level was found to be just on the way toward localization. The difference in excitation energies is not large, but the C_1 result is closer to experiment, consistent with the class II character assigned above on the basis of solvent shifts.

It should be noted again (cf. Computational Details) that the quantitative agreement of the TDDFT excitation energies with experiment depends on the chosen solvent model, and more work will have to be invested in examining how the parameters of the solvent model affect the excitation energies. Furthermore, the continuum solvent models used involve only the static dielectric constant. It is conceivable that more detailed future evaluations might have to deal with the different time scales of solvent relaxation. This discussion is outside the scope of the present work (see, e.g., refs 69 and 70).

A last point should be noted regarding the computed IV-CT excitation energies. As shown above, it is not trivial to arrive at the correct localized or delocalized structure, and due to the large solvent dependence of charge localization, gas-phase calculations are clearly inadequate in this context. In view of the appreciable dependence of the IV-CT excitation energies on the quality of the optimized input structure, the often-found short-cut methods that use gas-phase optimized ground-state structures and include solvent effects only in the TDDFT calculation are clearly inappropriate and discouraged.

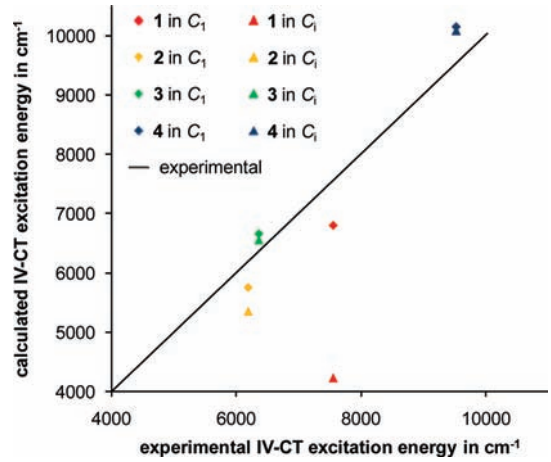

Figure 6. IV-CT excitation energies obtained for **1**−**4** with 35% HF-like exchange in dichloromethane in both structure optimization and TDDFT computation. Perfect agreement with experiment is indicated by the diagonal line. Data for unsymmetrical structures (C_1) and symmetrical structures (C_i) are provided.

5. Conclusions

The present systematic study of ground-state structures and properties, as well as IV-CT transition energies, of a series of organic mixed-valence (MV) radical cations close to the class II/III borderline has provided important insights that may bear on the computational description of organic (or even inorganic) MV systems in general. First of all, we find a strikingly large influence of solvent polarity on the positioning of such organic MV radical cations along the Robin−Day classification coordinate. Indeed, such classifications should generally be provided with explicit indication of the solvent used for the experimental characterization. The present results suggest that for systems close to the class II/III crossover, solvent polarity may indeed play the decisive role for the qualitative character of the MV cation. The importance of solvent polarity is even more significant due to the fact that these cations have to be studied in relatively polar solvents. So far, we have not considered the influence of the counterions.[7] Interionic interactions may also play a role, in particular regarding the crystal environment for solids. This has to be considered when interpreting X-ray structural results for such organic MV radical cations.

While the experimental evidence for the character of the title systems was partly contradictory and rather indirect, the combination of the computation of ground-state structure with the comparison of computed IV-CT excitation energies to experiment provided an unprecedentedly detailed classification and characterization. Among the four systems studied here, the phenylene-bridged, most strongly coupled example **4** has been found computationally to be a clear-cut class III case, irrespective of whether this is in the gas phase, or in different dielectric continuum solvent environments. All four cations **1**−**4** are class III in the gas phase or in a nonpolar solvent like hexane. In a more polar solvent like acetonitrile or dichloromethane, at least **1** and **2** exhibited symmetry breaking with hybrid functionals at moderate exact-exchange admixtures of about 35%. Analysis of ground- and excited-state data for the diphenylbutadiyne-bridged system **1** indicates clearly that in this case the symmetry breaking is real, and the compound is on the class II side both

in dichloromethane and in acetonitrile. This contrasts to artificially induced charge localization observed at very high exact-exchange admixtures in the gas phase or in hexane solution. The diphenylethyne-bridged compound **2** is closest to the class II/III border in acetonitrile and dichloromethane, but could be characterized as class II based on the solvent dependence of the IV-CT excitation energy. Finally, the computations on the biphenylene-bridged cation **3** suggest it to be on the class III side, but barely so.

The main result of this work is the proposal of a simple, practical protocol for reliable calculations on organic MV systems in general, based on hybrid functionals with about 35% exact-exchange admixture, together with suitable dielectric-continuum solvent models. The exact-exchange admixture of 35% is somewhat larger than in typical thermochemically optimized global hybrids like B3LYP. However, this does not seem to be a serious obstacle, as hybrid functionals with some dependence on local kinetic energy density may allow such elevated exact-exchange admixtures without sacrificing overall thermochemical accuracy. Alternatively, more sophisticated approaches such as range-separated hybrids or local hybrids may provide further improved accuracy. Eventually, for even more detailed evaluations, it may become necessary to consider also ion pairing in case of ionic MV systems. The present results and data set provide now a basis against which further methods may be compared and validated.

Acknowledgment. Dedicated to Prof. Paul von Ragué Schleyer on the occasion of his 80th birthday. This work has been supported by Deutsche Forschungsgemeinschaft within Graduiertenkolleg 1221 "Control of electronic properties of aggregated π-conjugated molecules". Johannes Buback is gratefully acknowledged for some initial calculations.

Supporting Information Available: Tables S1−S4 provide detailed ground-state structural data obtained at various computational levels. Tables S5−S8 give more detailed TDDFT results of excitation energies. Table S9 provides energies and Cartesian coordinates of those structures that have been used for the TDDFT calculations of Tables 5−8. Full citation of ref 66 is provided. This material is available free of charge via the Internet at http://pubs.acs.org.

JA9070859